New AOTF Technology for IR Hyperspectral Imaging

3 March 1998

Vladimir Pelekhaty, Xiaolu Wang
Brimrose Corp. of America
5020 Campbell Blvd.
Baltimore, MD 21236

Duane E. Paulsen
Air Force Research Laboratory
29 Randolph Road
Hanscom AFB, MA 01731-3010

ABSTRACT

We have developed a new Acousto-Optic Tunable Filter (AOTF) for implementation as a spectrally selective element for hyperspectral imaging applications in the NIR (.8 - 1.7 micron) and MWIR (2.5 - 4.5 micron) ranges of the optical spectrum. The new AOTF has high spectral resolution (about 3 cm^{-1}) and requires relatively low RF drive power. It has a broad acceptance angle and increased diffraction efficiency for enhanced optical throughput. In combination with a 2-D IR focal plane array the new AOTF allows for real time hyperspectral imaging of both self-emitting sources, such as astronomical objects or rocket exhaust plumes, and externally illuminated absorbing/reflecting specimens.

1.0 INTRODUCTION

Applications of the Acousto-Optic Tunable Filter (AOTF) for spectral imaging almost immediately followed the introduction of the AOTF itself [1-5] into the arsenal of spectrally selective devices, which greatly complemented the pre-existing prism, grating, interference filter, and etalon based spectroscopic instruments of the past. Such remarkable advantages of the AOTF as its robustness, absence of moving parts or components, high throughput and resolution as well as extremely fast spectral scanning capability have won for it numerous applications in spectroscopic measurements and spectral imaging [6-11].

REPORT DOCUMENTATION PAGE

Form Approved OMB No. 0704-0188

1. REPORT DATE (DD-MM-YYYY)	2. REPORT TYPE	3. DATES COVERED (FROM - TO)
03-03-1998	Conference Proceedings	xx-xx-1998 to xx-xx-1998

4. TITLE AND SUBTITLE
New AOTF Technology for IR Hyperspectral Imaging
Unclassified

5a. CONTRACT NUMBER
5b. GRANT NUMBER
5c. PROGRAM ELEMENT NUMBER

6. AUTHOR(S)
Pelekhaty, Vladimir ;
Wang, Xiaolu ;
Paulsen, Duane E. ;

5d. PROJECT NUMBER
5e. TASK NUMBER
5f. WORK UNIT NUMBER

7. PERFORMING ORGANIZATION NAME AND ADDRESS
Brimrose Corp. of America
5020 Campbell Blvd.
Baltimore, MD21236

8. PERFORMING ORGANIZATION REPORT NUMBER

9. SPONSORING/MONITORING AGENCY NAME AND ADDRESS
Director, CECOM RDEC
Night Vision and Electronic Sensors Directorate, Security Team
10221 Burbeck Road
Ft. Belvoir, VA22060-5806

10. SPONSOR/MONITOR'S ACRONYM(S)
11. SPONSOR/MONITOR'S REPORT NUMBER(S)

12. DISTRIBUTION/AVAILABILITY STATEMENT
APUBLIC RELEASE
,

13. SUPPLEMENTARY NOTES
See Also ADM201041, 1998 IRIS Proceedings on CD-ROM.

14. ABSTRACT
We have developed a new Acousto-Optic Tunable Filter (AOTF) for implementation as a spectrally selective element for hyperspectral imaging applications in the NIR (.8 - 1.7 micron) and MWIR (2.5 - 4.5 micron) ranges of the optical spectrum. The new AOTF has high spectral resolution (about 3 cm-1) and requires relatively low RF drive power. It has a broad acceptance angle and increased diffraction efficiency for enhanced optical throughput. In combination with a 2-D IR focal plane array the new AOTF allows for real time hyperspectral imaging of both self-emitting sources, such as astronomical objects or rocket exhaust plumes, and externally illuminated absorbing/reflecting specimens.

15. SUBJECT TERMS

16. SECURITY CLASSIFICATION OF:			17. LIMITATION OF ABSTRACT	18. NUMBER OF PAGES	19. NAME OF RESPONSIBLE PERSON
a. REPORT	b. ABSTRACT	c. THIS PAGE	Public Release	13	Fenster, Lynn lfenster@dtic.mil
Unclassified	Unclassified	Unclassified			19b. TELEPHONE NUMBER International Area Code Area Code Telephone Number 703767-9007 DSN 427-9007

For spectral imaging applications the AOTF is inserted in place of a fixed bandpass filter between the targeted object and the focal plane array as illustrated in Figure 1 [7-8]. An AOTF can be placed at the point in the optical path where the optical lens system forms an intermediate image of the target object (as shown in Figure 1a). In this case the filtering of the image itself will be performed directly. In an alternative implementation the AOTF can be placed where the optical system forms the spatial Fourier spectrum of the image, so its Fourier spectrum will be filtered instead, as shown in Figure 1b. In both cases the total number of resolvable fringes, N, is determined by the angular aperture of the AOTF, $\Delta\Theta$, its linear aperture, a, and the optical wavelength, λ [7]:

$$N = \Delta\Theta \; a \; / \; \lambda \qquad (1)$$

Obviously, either the image of the object or its Fourier spectrum (depending upon which of them is being filtered in the corresponding implementation of Figure 1a or Figure 1b) should fit within the linear aperture of the AOTF. Similarly all the light rays, which form the image or its Fourier spectrum, should be confined within the angular aperture of the same AOTF.

Acousto-Optic Tunable Filter

The performance of the AOTF is based on the anisotropic diffraction of light in a birefringent medium. It consists of a birefringent crystalline acousto-optic interaction medium with a piezoelectric transducer bonded to it. When the transducer is excited by an applied RF signal, an acoustic wave is launched into the acousto-optic crystal. The propagating acoustic wave produces a periodic modulation of the refractive index. This provides a moving phase grating which, under proper phase matching conditions, will diffract a portion of the incident light beam. Anisotropic acousto-optic diffraction couples the incident linearly polarized light wave, for example the ordinary wave, with the orthogonally polarized extraordinary diffracted optical wave. The bulk phase grating generated in the acousto-optic crystal by the acoustic wave provides both of the non-diagonal permittivity tensor elements required to couple the waves with the orthogonal polarization. The acoustic wave also provides the phase-matching between the two waves which sense different -- the ordinary n_o and extraordinary n_e -- refractive indices and, hence, propagate with different phase velocities. For a fixed acoustic frequency, only a certain narrow band around the central wavelength, which satisfies the phase-matching condition, will be cumulatively diffracted.

As the RF frequency is changed, the central wavelength of the optical passband is changed accordingly, so that the phase-matching condition is satisfied for a different wavelength. Because an AOTF rotates the polarization of the diffracted wave 90° with respect to the polarization of the incident wave, it can be sandwiched between the pair of crossed polarizers to separate the filtered out light from the incident one, as it is depicted in Figures 1a and 1b.

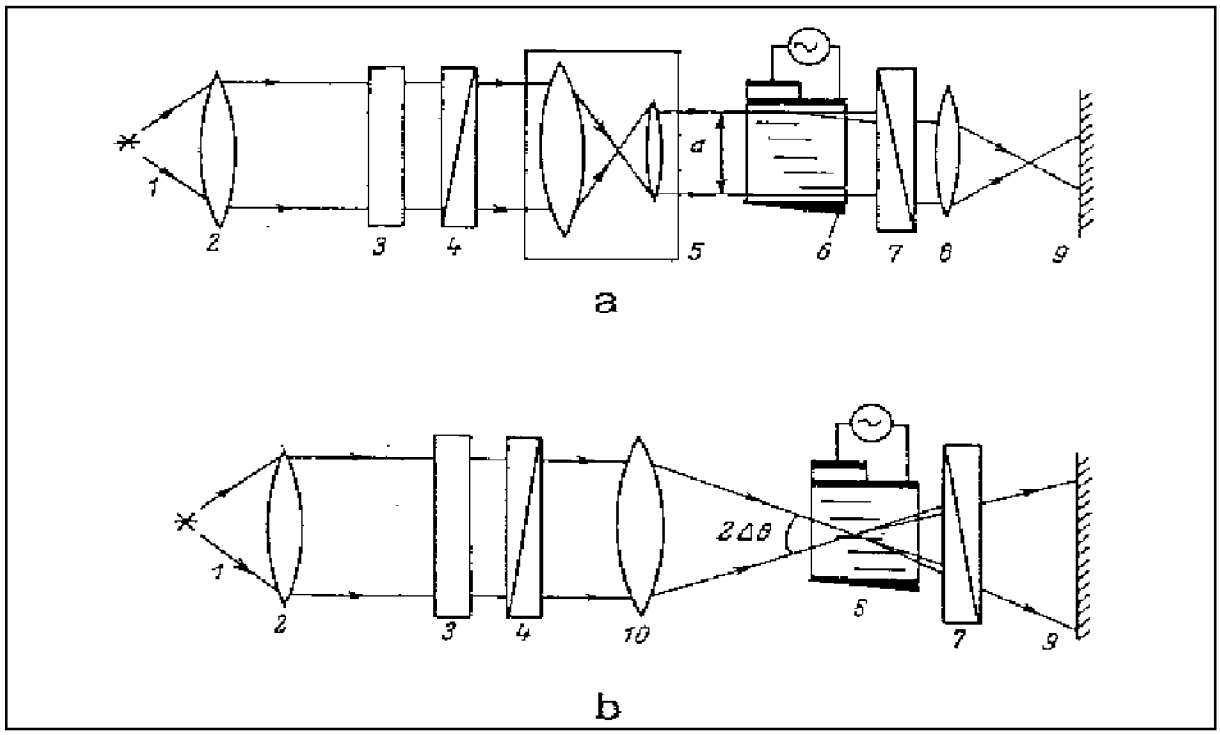

Figure 1. Optical arrangement for spectral image filtering:
a - filtering of the image directly; b - filtering of its Fourier spectrum.
1 - light source; 2 - condenser lens; 3 - transparency; 4 - polarizer; 5 - telescopic system; 6 - AOTF; 7 - crossed polarizer; 8 - objective lens;
9 - screen or 2-D sensor.

AOTFs generally fall into two categories depending upon the configuration of the acousto-optic interaction: non-collinear [4,5] or collinear [1-3] types.

Figure 2 illustrates the non-collinear AOTF which is most commonly made of tellurium dioxide (TeO_2), the preferred acousto-optic material in the visible and IR regions. Figure 2a shows the wave vector diagram for the phase-matching condition superimposed on the indicatrices of the ordinary and extraordinary refractive indices. Figure 2b shows a schematic realization of the non-collinear AOTF. The distinctive feature of the non-collinear AOTF is that the wave vectors of the ordinary and extraordinary optical waves form a triangle together with the wave vector of the phase-matching acoustic wave.

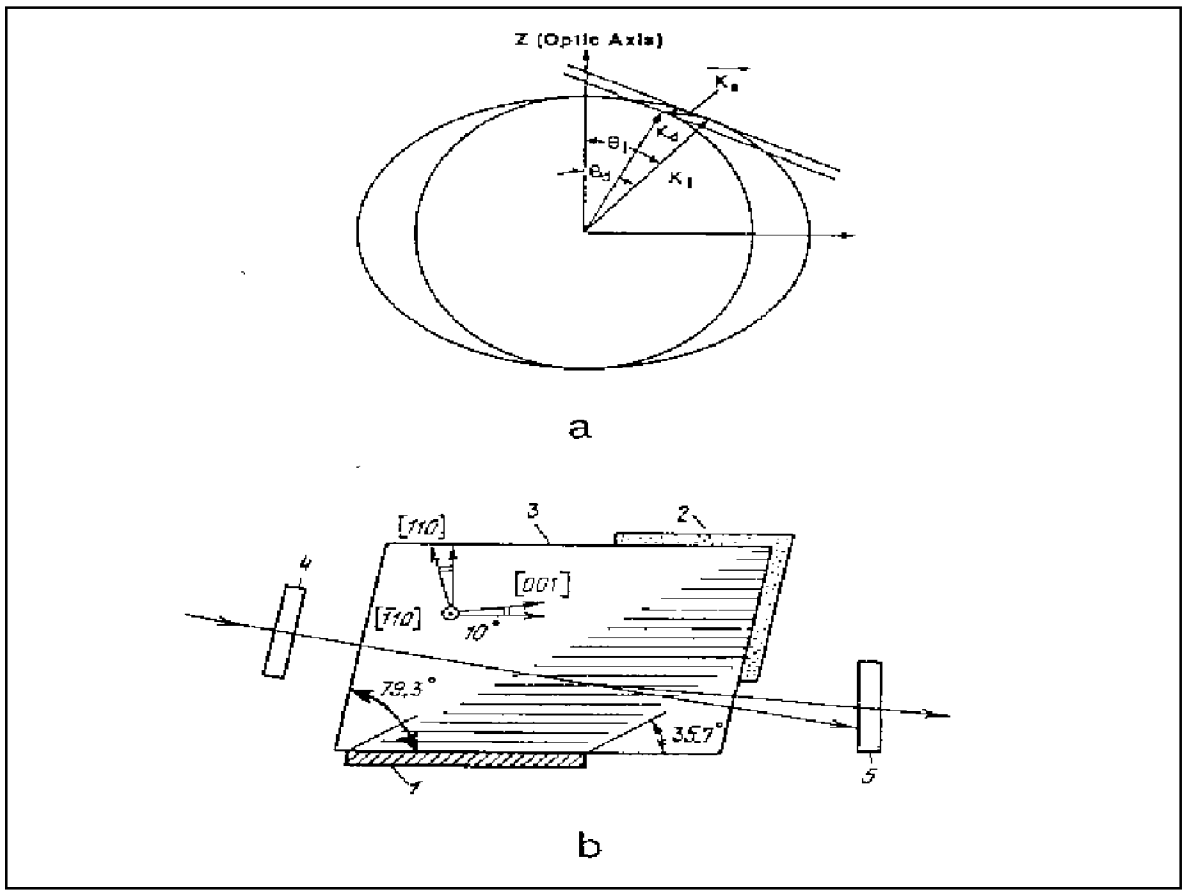

Figure 2. Non-collinear AOTF using tellurium dioxide crystal.
a - Wave vector diagram; b - Example of non-collinear AOTF [4].
1 - piezoelectric transducer; 2 - sound absorber; 3 - tellurium dioxide crystal;
4 - polarizer; 5 - analyzer.

This accounts for the different angular directions of incident and diffracted waves and in their spatial separation. The separation angle is typically a few degrees and, to the advantage of the non-collinear configuration, permits the operation of a non-collinear AOTF without the use of polarizers.

From the phase-matching triangle it is possible to obtain a tuning relation between the center frequency of the acoustic wave, f, and the optical passband center wavelength [4]:

$$f = V \Delta n \left(\sin^4\Theta + \sin^2 2\Theta \right)^{1/2} / \lambda \qquad (2)$$

where Θ is the polar angle of the light propagation, V is the acoustic velocity, and $\Delta n = n_e - n_o$ is the optical birefringence. As follows from the above equation, the wavelength of the light that is selected by acousto-optic diffraction can therefore be varied simply by changing the applied RF frequency.

An important parameter of an AOTF is the required drive power. The peak transmission of an AOTF is given by [15]

$$T = \sin^2(\pi^2 M_2 P L^2 / 2 \lambda^2)^{1/2} \quad (3)$$

where P is the acoustic power density, M_2 is the acousto-optic figure of merit, and L is the length of acousto-optic interaction. The peak transmission versus the RF drive power reaches 100% when $P = P_{100\%} = \lambda^2 / 2 M_2 L^2$. To achieve 50% transmission, it takes only a quarter of $P_{100\%}$.

Another important parameter of an AOTF is its spectral resolution. It is especially essential for spectral imaging applications, because, as it was shown in [10], the non-monochromatic output of the AOTF is being dispersed by the acousto-optic phase grating, which causes the spectral blurring of the filtered image in the direction of the acousto-optic deflection, while the image in the direction perpendicular to the plane of deflection is undistorted.

The wavelength resolution of an AOTF can be calculated by the formula [15]

$$\Delta\lambda = 0.9 \lambda^2 / L \Delta n \sin^2\Theta \quad (4)$$

A disadvantage of the non-collinear AOTF is that optical beam, as shown in Figure 2b, intersects the acoustic column at relatively steep angle, which results in the interaction length L being equal to only about half of the length of the transducer and, hence, can not take advantage of the full length of the crystal. This means that the spectral resolution is less than might be realized if the entire length of the crystal could be utilized. In addition, if the spectral response peak of the non-collinear AOTF is too broad it will further diminish the spatial resolution of the non-collinear AOTF through the aforementioned spectral blurring.

A collinear AOTF, which is shown in Figure 3, does not have this drawback, because the optical and acoustic beams are co-propagating along the same direction, usually perpendicular or close to perpendicular to the optical axis. In this case the length of the acousto-optic interaction does not depend on the size of the transducer and is as long as the physical length of the available crystal. Unfortunately, the collinear regime is unrealizable in tellurium dioxide because its acousto-optic figure of merit M_2 is equal to zero for the optical propagation direction perpendicular to the optical axis, as it is shown in Figure 4.

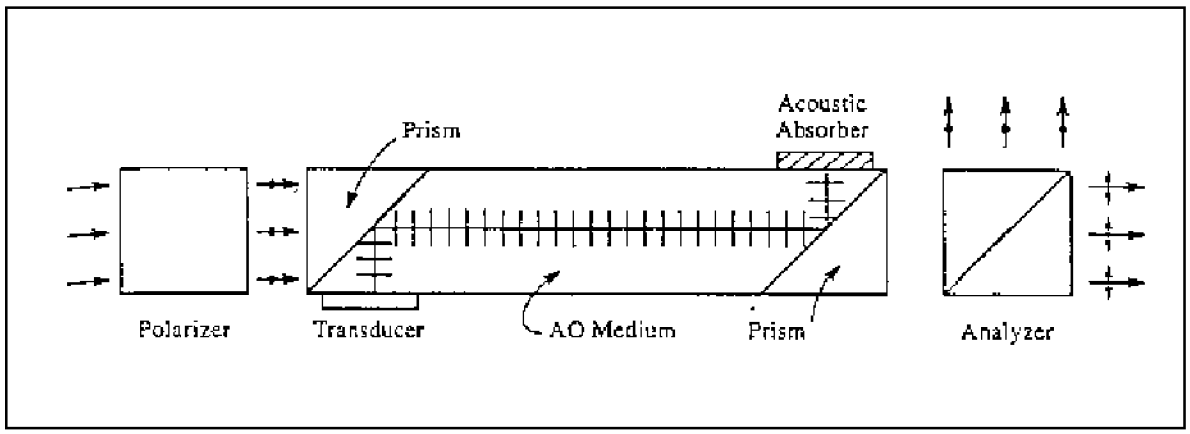

Figure 3. Collinear AOTF.

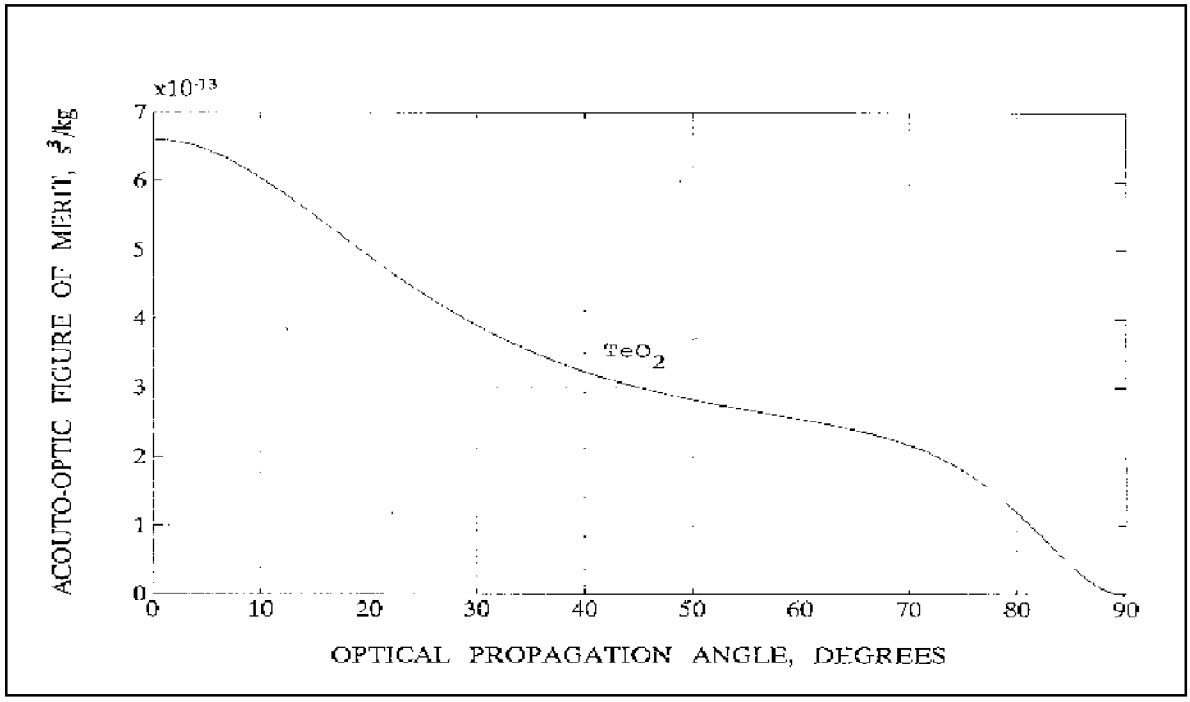

Figure 4. Acousto-optic figure of merit for non-collinear AOTF in tellurium dioxide

Lithium niobate is another high quality optical crystal [12], which permits the operation of the collinear type of acousto-optic diffraction [1,2]. Even if its acousto-optic figure of merit, shown in Figure 5 as a function of the polar angle of the optical propagation direction, is much lower than that of tellurium dioxide, the effect of the longer collinear acousto-optic interaction region will compensate for it and provide significant diffraction efficiency at a moderate RF drive power.

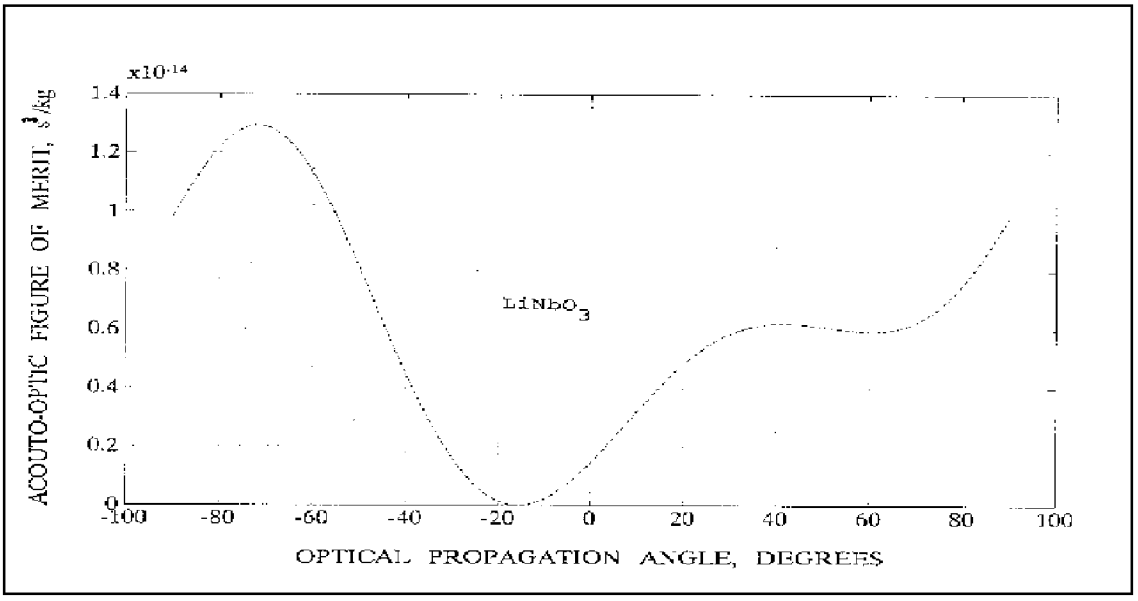

Figure 5. Acousto-optic figure of merit for AOTF in lithium niobate

New collinear lithium niobate AOTF

The sketch of the newly designed AOTF is shown in Figure 6. The acoustic wave is launched into the crystal by the piezoelectric transducer bonded to the left slope of the V-shaped cut-out in the lithium niobate crystal [14]. The launched shear acoustic wave hits the optical window and gets reflected from the free crystal-air interface. The reflected acoustic wave co-propagates with the light wave along the length of the device at an angle Θ = 86° with respect to the optical axis [13] and gets reflected again at the output optical window onto the acoustic absorber. Both input and output optical windows are brewsterized to insure zero Fresnel reflections for both incident and filtered out optical beams.

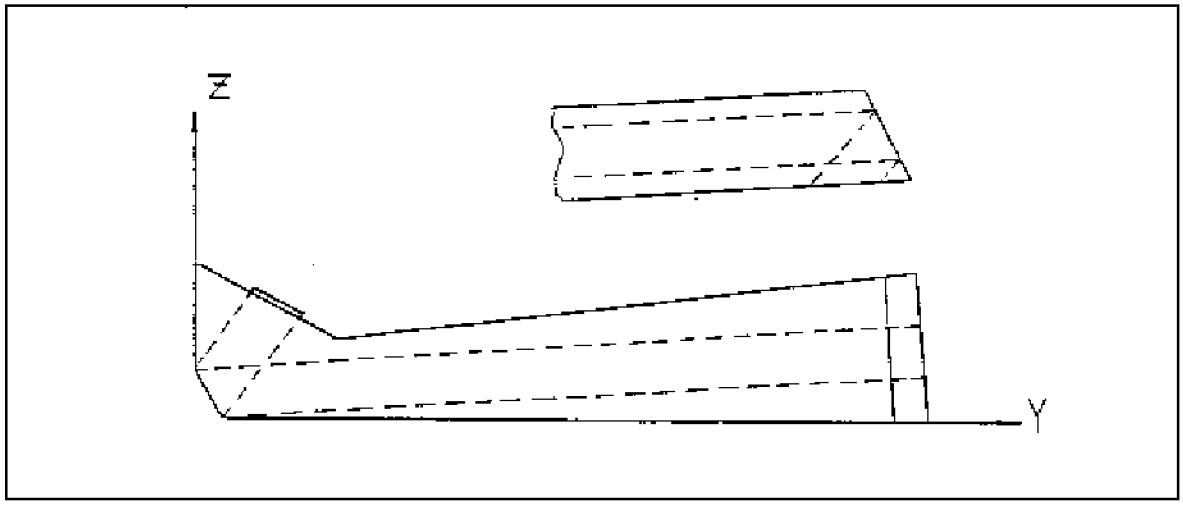

Figure 6. Sketch of the newly designed lithium niobate AOTF.

Based on expression (2) with Θ = 86°, the tuning relation between the frequency of the acoustic wave and the center wavelength of the filtered light in NIR was calculated. The resulting tuning curve is plotted in Figure 7. It shows that to cover the range of sensitivity of an InGaAs photodetector 0.8 - 1.7 micron, the frequency of the acoustic wave should vary between 170 MHz and 390 MHz.

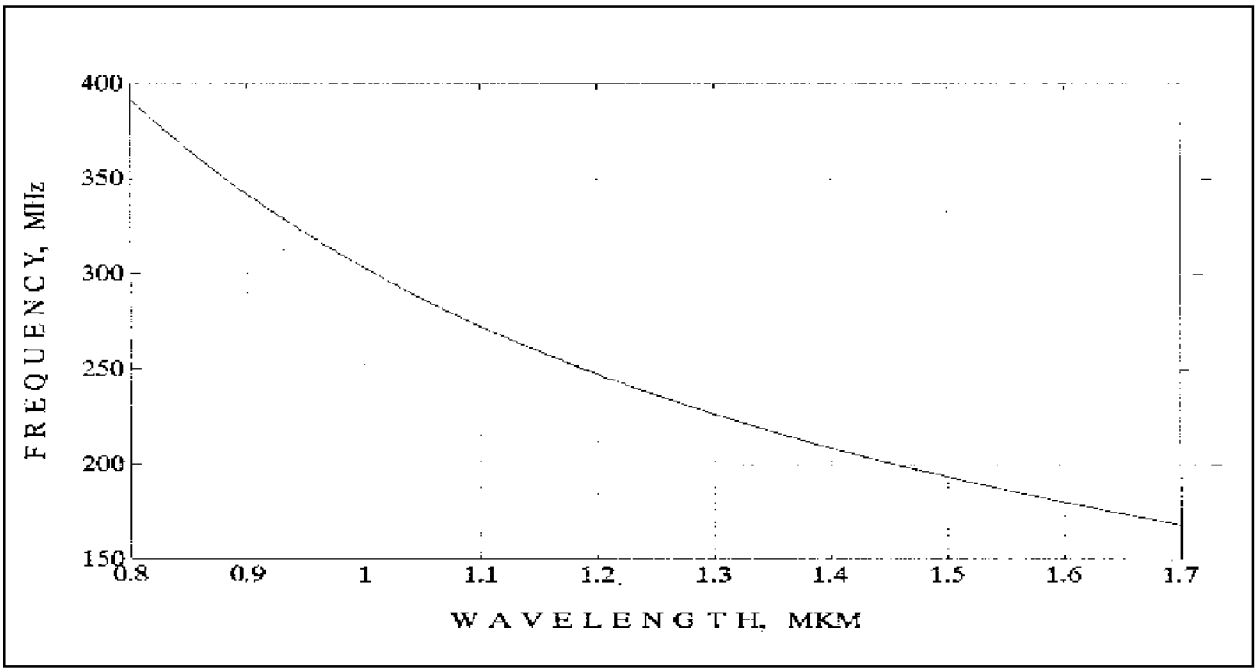

Figure 7. Tuning characteristics of the newly designed lithium niobate AOTF.

The interaction length of this AOTF is equal to 75 mm, which is almost the whole physical length of the 80 mm long boule. This value is an order of magnitude higher than the interaction length in the conventional non-collinear AOTF. As follows from equation (4) for the resolution of the AOTF with Θ = 86° and L = 75 mm, the expected resolution of the new collinear AOTF should be an order of magnitude higher than that of the conventional non-collinear one. The calculated resolution of the new designed AOTF with a 75 mm long interaction length is plotted in Figure 8 versus wavelength for the same NIR range. It varies between 1.2 Å for 0.8 micron and 5.7 Å for 1.7 micron. The extremely high spectral resolution of the new AOTF eliminates the influence of the spectral blurring of the filtered image [10]. Another benefit of the extremely high resolution of the new AOTF is in the potential applicability of it for the detection of fine spectral structures unresolvable for the conventional non-collinear AOTF.

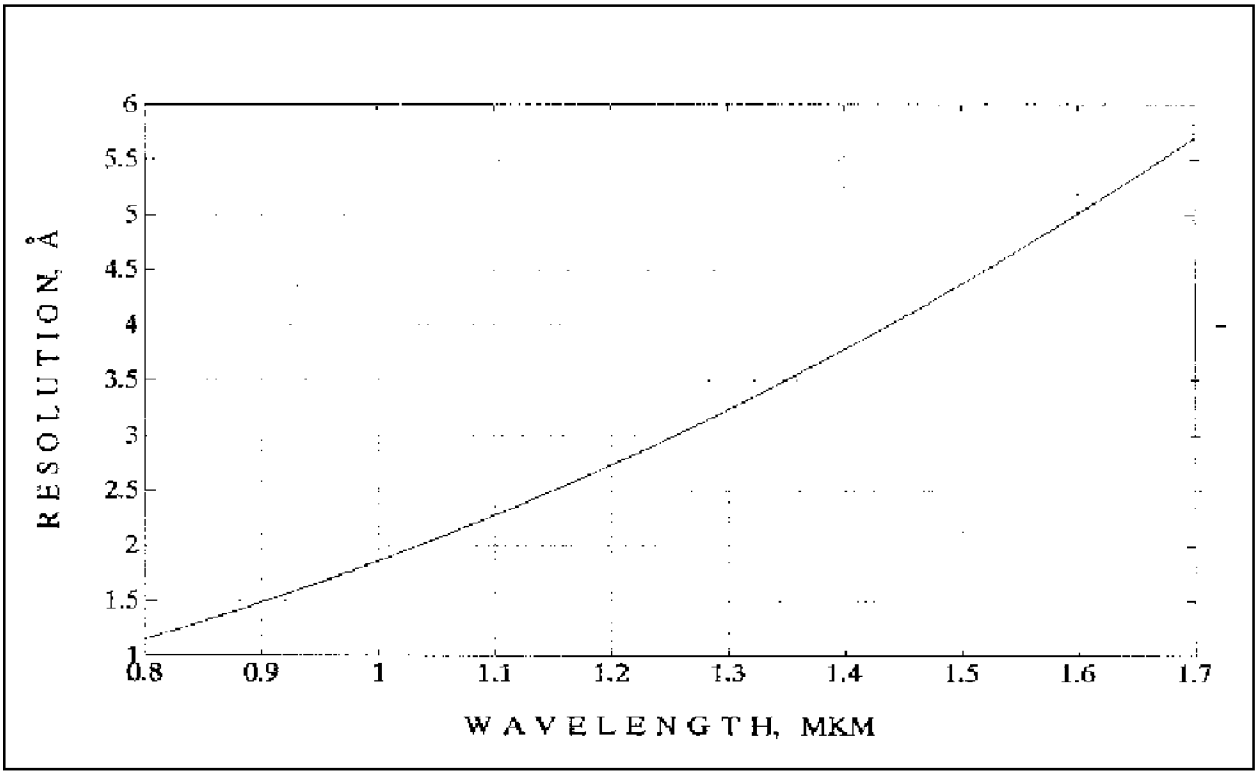

Figure 8. Calculated resolution of the newly designed AOTF with 3" long interaction.

These design parameters, such as the interaction length L = 75 mm, affect another important characteristic of the AOTF, its full external (in the air) acceptance angle, which can be calculated as

$$2\, n_o\, \Delta\Theta = 2\, n_o\, (\, \lambda\, /\Delta n\, L\,)^{1/2} \qquad (5)$$

As follows from expression (5), the acceptance angle of the AOTF decreases with the increase of the interaction length, but only as square root of it. The calculated dependence of the full external acceptance angle of the new AOTF on the filtered wavelength is plotted in Figure 9. It varies between 3.1° and 4.6° throughout the wavelength range. This would allow the new AOTF to provide both high throughput and, according to expression (1), a large number of resolvable fringes, i. e., high spectral resolution.

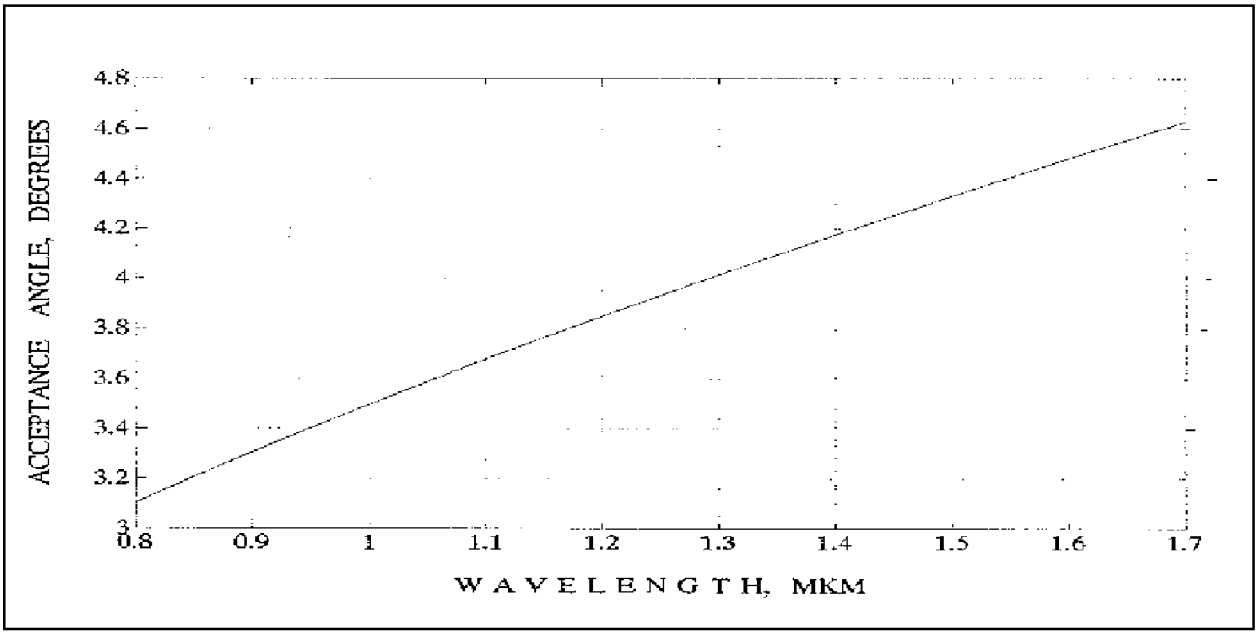

Figure 9. Calculated full external acceptance angle of the new AOTF.

Polarizing birefringent prisms made out of the same lithium niobate crystal (not shown in Figure 6) were attached to the optical windows. They are designed to compensate for the refraction and dispersion of the input and output optical beams at the angled optical crystal-to-air interfaces. In combination with the birefringent AOTF crystal itself these birefringent prisms serve as built-in polarizers, which spatially separate the diffracted optical beam from the incident optical beam and eliminate the need for external polarizers.

The piezoelectric transducer (and, correspondingly, the linear aperture of the AOTF) has an area about 0.5 cm^2 and was thinned down to 9 micron, which makes it resonate at 250 MHz. The resulting clamped capacitance of the transducer reached a value of about 2000 picofarads. The impedance of a capacitor that large at the resonance frequency is less than 0.5 ohm. This low impedance has to be matched to the standard 50 ohm generator over the more than an octave of RF frequency required for the broad wavelength tuning range. To accomplish this, a proprietary impedance matching technique was developed and implemented.

The frequency range of the fabricated AOTF covered more than octave (170-354 MHz), with a corresponding wavelength tuning range of 0.88 - 1.7 micron. This wavelength range coincides with the sensitivity range of the InGaAs photodetector. The diffraction efficiency of the new AOTF was measured with 2 Watts of RF power applied to the AOTF. The measured test data are plotted in Figure 10 versus RF frequency. The maximum diffraction efficiency of 50% was achieved at the frequency corresponding to the peak wavelength 1.1 micron. Such a relatively high diffraction efficiency was achieved due to the long interaction length, which compensated (as shown by equation (3) for the much lower figure of merit of the lithium niobate, compared to tellurium dioxide.

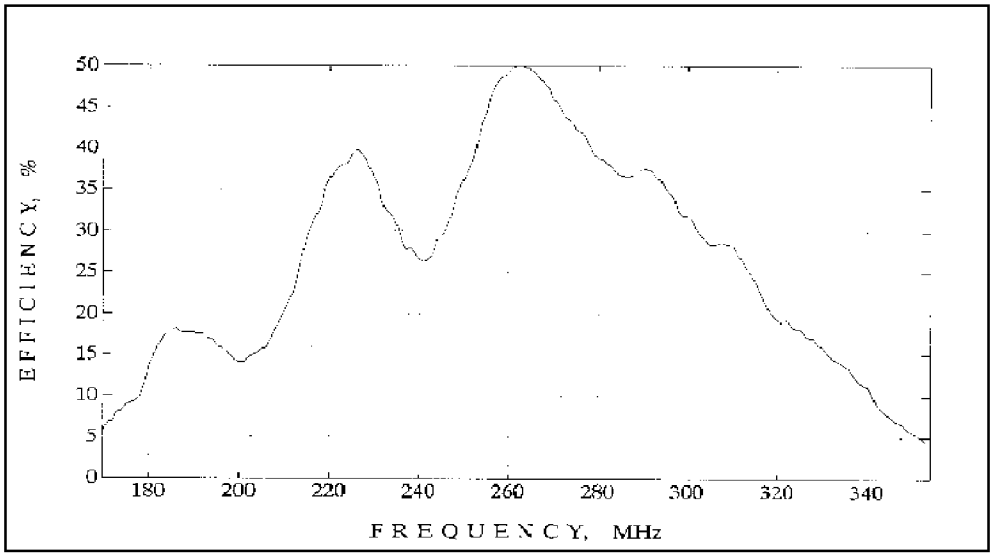

Figure 10. Measured diffraction efficiency of the new collinear AOTF.

The wavelength resolution of the new AOTF was measured by scanning over a narrow line of a He-Ne laser. Figure 11 shows the response of the AOTF at 1.523 microns. The full width at half maximum (FWHM) wavelength resolution, $\Delta\lambda$, was 6Å, which is somewhat larger than the calculated value of 4.5Å. This discrepancy is probably due to the spoiling influence of the slight inhomogeniety of the $LiNbO_3$ boule. The slight broadening of the spectral response of the AOTF does not impair its utility for high resolution hyperspectral imaging and spectral analysis. This spectral broadening can be further reduced by more thorough control of the optical quality of the lithium niobate crystalline material.

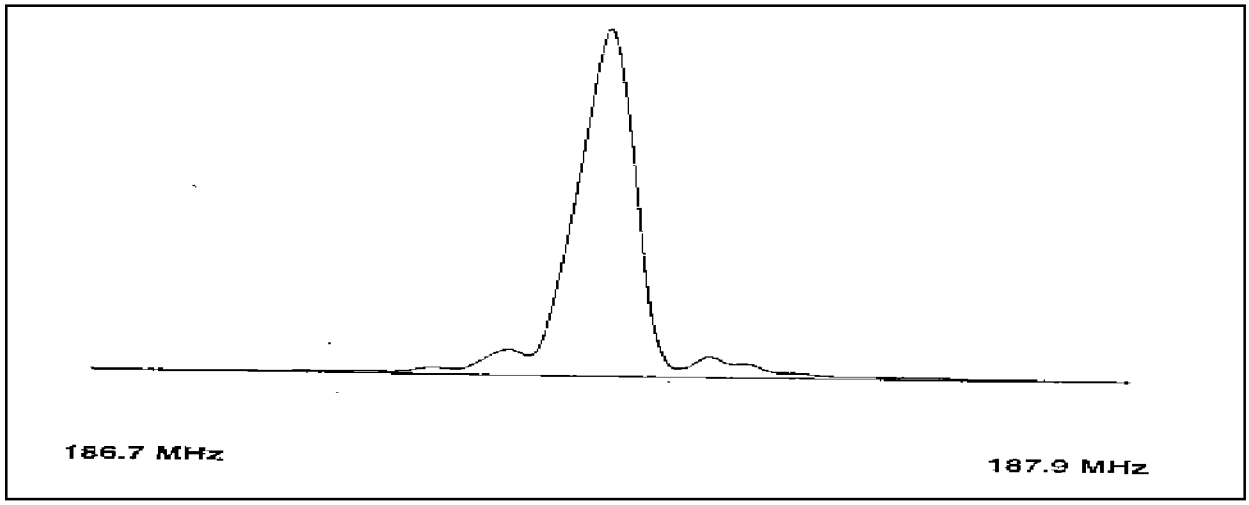

Figure 11. Response curve of the new AOTF for the 1.523 micron He-Ne laser.

Finally, we can evaluate the total number of the resolvable pixels, which can be imaged through the new AOTF. This number is equal

to *NxN*, where *N* is number of the resolvable fringes, calculated by equation (1). The results of the calculated number of resolvable fringes for the AOTFs with the apertures 5 mm x 5 mm, 7 mm x 7 mm, and 10 mm x 10 mm are shown in Figure 12 versus wavelength. The calculations show that an AOTF with 5 mm x 5 mm aperture would require a 2-D array with more than 128x128 pixels, while an AOTF with 10 mm x 10 mm aperture would need more than 256x256 pixels to successfully realize their spatial imaging capabilities. These numbers are within the range of commercially available 2-D focal plane arrays. The new AOTF is fully capable of providing high spectral resolution as well as high spatial resolution.

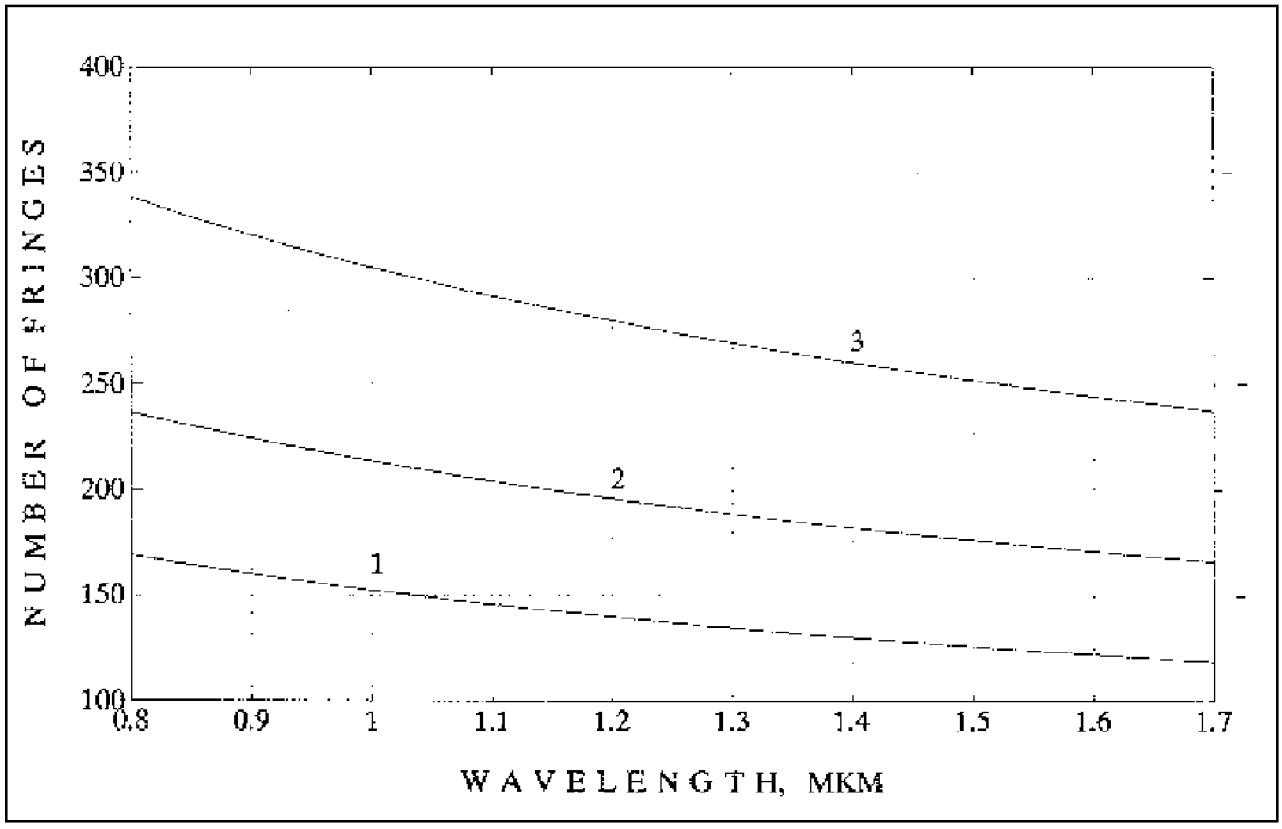

Figure 12. Calculated number of resolvable fringes for the AOTFs with different
apertures: 1 - 5 mm x 5 mm; 2 - 7 mm x 7 mm; 3 - 10 mm x 10 mm.

SUMMARY

We have described progress in developing AOTF technology that would be suitable for making spectral IR measurements of complex scenes. Our goal has been to develop a new imager and at the same time to explore the limits of the AOTF as a spectral imager. With the improved spectral resolution of this AOTF it is now possible to push the tradeoffs of AOTF based instrument design significantly further than was previously possible.

REFERENCES

1. S. E. Harris and R. W. Wallace, " Acousto-Optic Tunable Filters," J. Opt. Soc. Am. **59,** 744(1969).

2. S. E. Harris, S. T. K. Nieh, and D. K. Winslow, " Electronically Tunable Acousto-Optic Filter," Appl. Phys. Lett. **15,** 325 (1969).

3. I. C. Chang, " Tunable Acousto-Optic Filter Utilizing Acoustic Beam Walkoff in Crystal. Phys. Lett. **25,** 323 (1974).

4. I. C. Chang, " Noncollinear Acousto-Optic Filter with Large Angular Aperture," Appl. Phys. Lett., **25,** 370 (1974).

5. I. C. Chang, " Analysis of the Noncollinear Acousto-Optic Tunable Filter," Electron. Lett. **11,** 617 (1975).

6. D.L. Hecht, I. C. Chang, and A. Boyd, " Multispectral Imaging and Photomicrography Using Tunable Acousto-Optic Filters," OSA Annual meeting, Oct. 1975, Boston, Mass.

7. I. B. Belikov, G. Ya. Buimistryuk, V. B. Voloshinov, L. N. Magdich, M. I. Mit'kin, and V. N. Parygin, " Acoustooptic Image Filtering," Sov. Tech. Phys. Lett. **10,** 517 (1984).

8. Yu. K. Kalinnikov and L. Ya. Statsenko, " Use of Acoustooptical Filters for Image Filtration," Sov. Phys. Tech. Phys. **34,** 1050 (1989).

9. I. Kurtz, R. Dwelle, and P. Katzka, " Rapid Scanning Spectroscopy Using an Acousto-Optic Tunable Filter," Rev. Sci. Instrum. **58,** 1996 (1987).

10. D. R Suhre, M. Gottlieb, L. H. Taylor, and N. T Melamed, " Spatial Resolution of Imaging Noncollinear Acousto-Optic Tunable Filters," Opt. Eng. **31,** 2118 (1992).

11. D. A Glenar, J. J. Hillman, B. Saif, and J. Bergstralh, " Acousto-Optic Imaging Spectropolarimetry for Remote Sensing," Appl. Opt. **33,** 7412 (1994).

12. R. S Weis and T. K. Gaylord, " Lithium Niobate: Summary of Physical Properties and Crystal Structure," Appl. Phys. A **37,** 191 (1985).

13. J. A Kusters, D. A Wilson, and D. L. Hammond, " Optimum Crystal Orientation for Acoustically Tuned Optical Filters," J. Opt. Soc. Am. **64,** 434 (1974).

14. A. Sivanayagam and D. Findlay, " High Resolution Noncollinear Acousto-Optic
Filters with Variable Passband Characteristics: Design," Appl. Opt. **23,** 4601 (1984).

15. J. Xu and R. Stroud, " Acousto-Optic Devices," John Wiley & Sons, 1992.

.